Turkish Journal of Electrical Engineering & Computer Sciences

http://journals.tubitak.gov.tr/elektrik/

Research Article

Turk J Elec Eng & Comp Sci
(2016) 24: 3877 – 3897

doi:10.3906/elk-1410-73

Steady state analysis of a three phase indirect matrix converter fed 10 HP, 220 V, 50 Hz induction machine for efficient energy generation

Damian NNADI[1,*], **Crescent OMEJE**[2]
[1]Department of Electrical Engineering, University of Nigeria, Nsukka, Nigeria
[2]Department of Electrical Engineering, University of Port Harcourt, Rivers State, Nigeria

Received: 13.10.2014 • **Accepted/Published Online:** 21.06.2015 • **Final Version:** 20.06.2016

Abstract: The matrix converter or pulse width modulated frequency changer, invented in the mid-1980s, is a direct power conversion device that can generate a variable voltage and frequency from a variable input source. Industrially, it is applied in adjustable speed control of induction motor drive, power quality conditioner, and traction applications. The aim of this paper is to evaluate the steady state characteristic behavior of an induction machine in terms of its speed and torque when driven by a three phase indirect matrix converter at reduced harmonics. Similarly, projecting an AC-AC matrix converter that ensures a uniform synchronization in frequency and voltage supplies between the three phase wound rotor machine and the transformer's grid voltage supply is discussed in the Scherbius scheme. The different methods of torque calculations pertaining to some selected machine circuit diagrams are presented for comparison and analysis. Emphasis on the torque-speed characteristics of the machine at varied resistance and slip values were graphically analyzed in MATLAB to determine the degree of torque-speed dependence on the rotor resistance and slip. The overall behavior of the machine under motoring, plugging, and regenerative modes was considered in this work, while a detailed Simulink modeling of an indirect matrix converter on the Scherbius drive scheme is also presented for further analysis.

Key words: Indirect matrix converter, induction machine drive, steady state torque-speed characteristics, Scherbius drive, Simulink modeling

1. Introduction

The matrix converter or pulse width modulated frequency changer, invented in the mid-1980s, is a direct power conversion device that can generate a variable voltage and frequency from an AC power source to an AC output of equal or higher magnitude. The matrix converter as an AC to AC energy conversion device is commonly exploited in many recent industrial applications such as adjustable speed motor drives, power quality conditioners, and traction applications [1–4].

Appreciable demand for AC to AC energy conversion has enormously depended on distributed generation (DG), where a sizeable number of decentralized sources need to be tied to the utility or distribution grid. Commonly known examples of matrix converter applications include wind energy conversion systems, diesel generators, slip energy recovery schemes of induction motors (Scherbius drives), and microturbines [5]. Therefore, with respect to the aforementioned distributed generation, direct connection of the source (three phase supply) to the distribution grid is usually impracticable because of mismatches in the amplitude of voltage due to line harmonics and uneven synchronization of frequency between the three phase supply and the grid

*Correspondence: damian.nnadi@unn.edu.ng

(usually varying at the source but fixed at the grid terminal). To avert this stated anomaly, proper AC to AC power electronic converters are therefore connected for interfacing the source to the grid for proper frequency synchronization [6]. In achieving this prime objective, 2 alternative converters, the back to back converter (B2B) and a detailed Simulink modeling of the indirect matrix converter (IMC) on the Scherbius drive scheme, are explained here with pertinence to their operational efficiency.

In its earliest form, the matrix converter was usually drawn like a 3×3 matrix with a total of 9 bidirectional or 18 unidirectional switches. Such an arrangement provides full bidirectional power flow flexibility, which may not be useful for DG, where power is flowing unidirectionally from the source to the distribution grid [7,8].

Matrix converters are classified into direct and indirect matrix converters. Although there exists the sparse matrix converter, which could have been a third type, research analysis has proven that this topology is almost analogous to the indirect matrix converter [9].

2. Direct matrix converter

The direct matrix converter topology consists of n and p bidirectional switches connecting the n-input path to the p-output path, aimed at providing a direct power conversion [10]. An n-input phase and p-output phase of an abridged direct matrix converter is shown in Figure 1a, while a detailed diagram is presented in Figure 1b, with the ideal switch symbol representing the bidirectional switch as shown in Figure 1b.

The direct matrix converter topology has the following attractive features:

- It has sinusoidal input current and output voltage.
- It employs bidirectional switches that enable the regeneration of energy to the source.
- It enables the adjustment of the input power factor of the converter in spite of the load type connected. This implies that unity power factor is easily achievable.
- There is no intermediary DC energy storage link. Therefore, the cost and size of the converter is relatively reduced.

The major limitation of the direct matrix converter is the commutation difficulties. The three phase AC to AC direct matrix converter topology is prone to commutation failure, which could be either a short circuit or an open circuit fault of the switching devices. The short-circuit fault occurs when 2 bidirectional switches from 2 phase lines are turned on, resulting in current spike across the load. An open-circuit fault occurs when the switches are turned off, which results in the absence of a conducting path for the inductive load current, thus causing a large voltage spike that may destroy the switches. As a corrective measure, bidirectional switches of a two to three phase input line cannot be turned on or off simultaneously, but should at all times have a definite conduction time and dead band (dead beat).

The above analogy is illustrated by considering a two phase input to single phase output part of the converter as shown in Figures 2a–2e, with the switching pattern drawn and presented in Table 1. At the instant of initial conduction, the bidirectional switches in phase A are turned on, while the switches in phase B are turned off.

Assume the load current flows in the positive direction as shown in Figure 2a. The switch S_{a1} is turned on with S_{a2}, which is in conformity with Table 1, until half cycle duration is attained before turning off S_{a2}, which at this time has zero conduction current, as proven by Table 1 and Figure 2b. After a given time delay

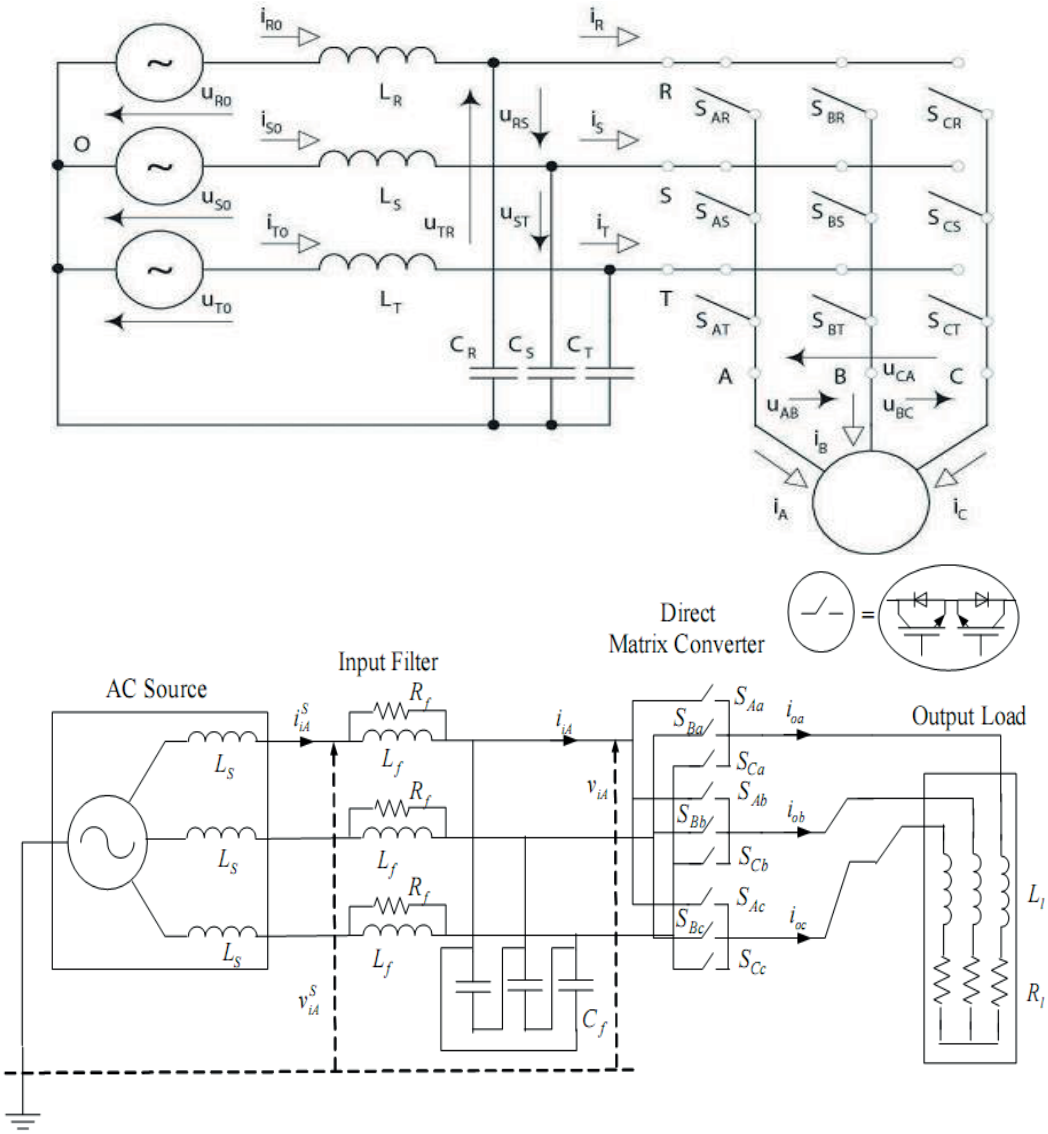

Figure 1. a. Abridged diagram of direct matrix converter. b. Full diagram of a direct matrix converter.

(dead beat), S_{b1} is turned on, thereby conducting a load current across the load as shown in Figure 2c. As a result of forced commutation emanating from reverse load current, S_{a1} is turned off by this forced commutation, as shown in Figure 2d, while S_{b1} maintains its load current conduction after a period of $\frac{\pi}{3}$ before S_{b2} is set into conduction, thus providing a reverse direction for the load current as presented in Figure 2e [10].

Similarly, a three phase input to a single phase output connection follows the same rule with a slight modification in the switching pattern, as presented in Table 2. The initial time delay or dead beat is derived from Eq. (1) while the actual control delay angle chosen in this analysis is $\alpha = \frac{\pi}{3}$.

$$\omega t_a = \pi \left(\frac{1}{2} - \frac{1}{N_p} \right), \tag{1}$$

Here, N_p stands for the number of pulses of the converter, $N_P \geq 2$.

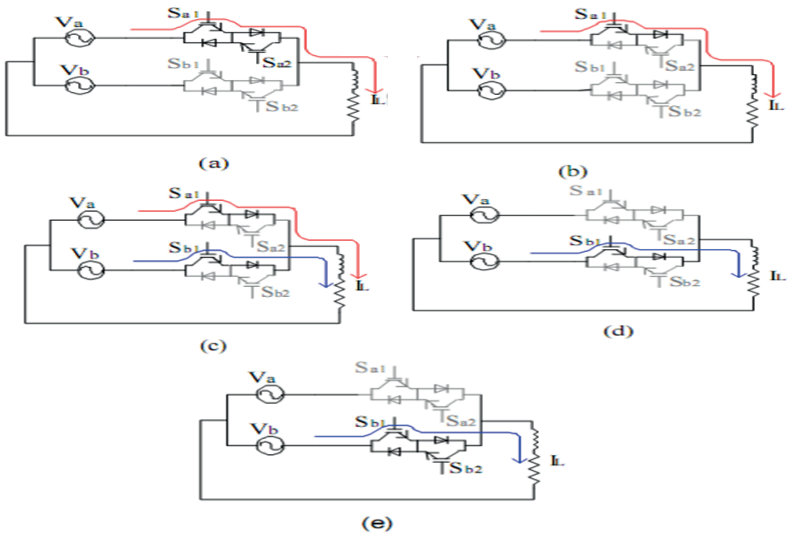

Figure 2. A two phase input to single phase output switching path (a–e).

Table 1. Switching signal of Figures 2a–2e.

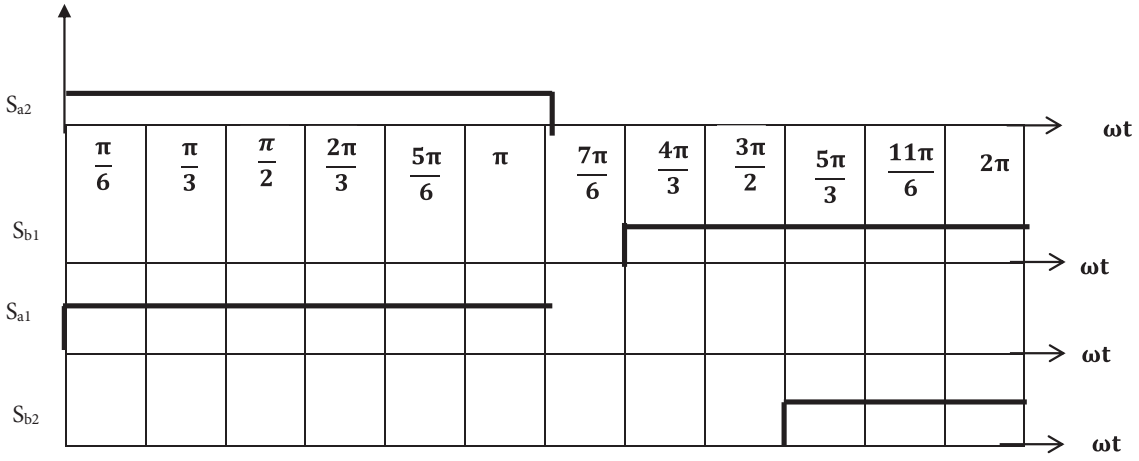

Figures 3a–3f depict the circuit diagrams that illustrate the current direction as well as the conducting bidirectional switches, which are drawn in dark lines, while faint lines represent the nonconducting switches. The conduction path is indicated by the arrow projection.

Summarily, the bidirectional switching combination modes for a three phase direct matrix converter with reference to Figure 3a above is effectively achieved by the following group classification:

- **Group 1**: This consists of a switching combination where the 3 different input phases of the converter are connected to each output phase.
- **Group 2**: This consists of those switching combinations where only 1 input phase is connected to 2 output phases, with the third output phase connected to a different input phase.

Table 2. Switching signal of Figures 3a–3f.

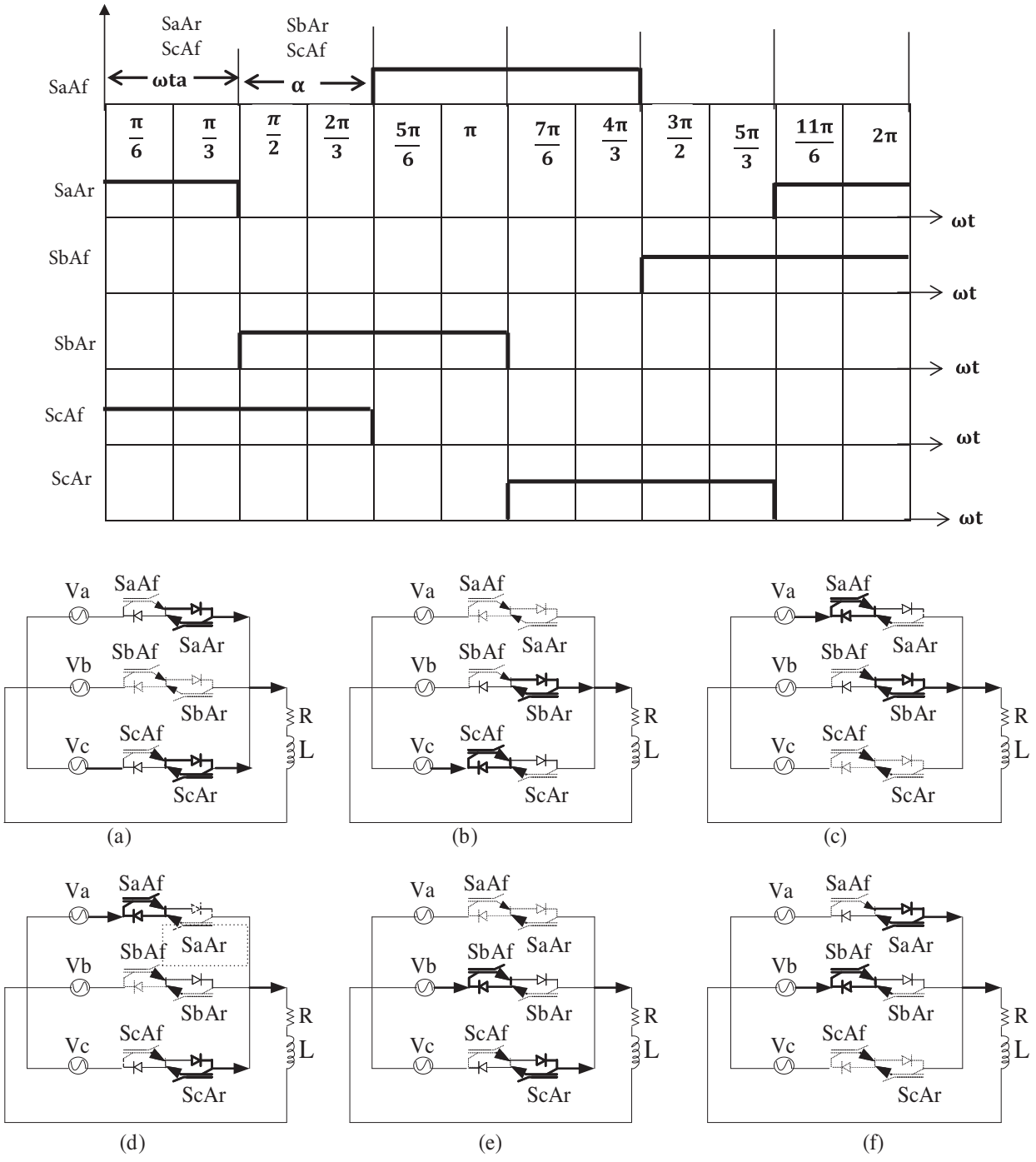

Figure 3. A three phase input to single phase output switching path (a–f).

- **Group 3**: In this third group, all 3 output phases are shorted by 1 input phase; in other words, all 3 output phases are connected to 1 input phase.

The switching combinations for these classified groups are presented in Table 3 for clarity.

Table 3. Switching combinations for input and output phase connection of Figure 1a.

Group	State No.	Input/output connection			Switching functions for input/output phase connection								
		A	B	C	S_{AR}	S_{BR}	S_{CR}	S_{AS}	S_{BS}	S_{CS}	S_{AT}	S_{BT}	S_{CT}
Group 1	1	R	S	T	1	0	0	0	1	0	0	0	1
	2	R	T	S	1	0	0	0	0	1	0	1	0
	3	S	R	T	0	1	0	1	0	0	0	0	1
	4	S	T	R	0	1	0	0	0	1	1	0	0
	5	T	R	S	0	0	1	1	0	0	0	1	0
	6	T	S	R	0	0	1	0	1	0	1	0	0
Group 2	7	R	T	T	1	0	0	0	0	1	0	0	1
	8	S	T	T	0	1	0	0	0	1	0	0	1
	9	S	R	R	0	1	0	1	0	0	1	0	0
	10	T	R	R	0	0	1	1	0	0	1	0	0
	11	T	S	S	0	0	1	0	1	0	0	1	0
	12	R	S	S	1	0	0	0	1	0	0	1	0
	13	T	R	T	0	0	1	1	0	0	0	0	1
	14	T	S	T	0	0	1	0	1	0	0	0	1
	15	R	S	R	1	0	0	0	1	0	1	0	0
	16	R	T	R	1	0	0	0	0	1	1	0	0
	17	S	T	S	0	1	0	0	0	1	0	1	0
	18	S	R	S	0	1	0	1	0	0	0	1	0
	19	T	T	R	0	0	1	0	0	1	1	0	0
	20	T	T	S	0	0	1	0	0	1	0	1	0
	21	R	R	S	1	0	0	1	0	0	0	1	0
	22	R	R	T	1	0	0	1	0	0	0	0	1
	23	S	S	T	0	1	0	0	1	0	0	0	1
	24	S	S	R	0	1	0	0	1	0	1	0	0
Group 3	25	R	R	R	1	0	0	1	0	0	1	0	0
	26	S	S	S	0	1	0	0	1	0	0	1	0
	27	T	T	T	0	0	1	0	0	1	0	0	1

2.1. Indirect matrix converter

The direct AC-AC matrix converter topology discussed above has a simple modular structure and many attractive features. Nevertheless, the complexity of its modulation control strategy and its commutation problem prevent it from being used in industry. An alternative approach with a practicable solution was proposed in [11], where a two stage converter topology consisting of a three phase 6 bidirectional switched rectifiers and 6 unidirectional switched inverters separated from each other by a seemingly fictitious DC link labeled as p and n are incorporated together, as shown in Figure 4.

This composite converter with the abovementioned features is called an indirect matrix converter (IMC). It is of note that all the important features of the direct matrix converter topology, such as improved sinusoidal input current and voltage, bidirectional switching principle for the rectifier operation, a seemingly unity power factor, and absence of DC storage elements, are achieved by this IMC topology. In addition, this topology simplifies the complexity of modulation control and the inherent commutation problems associated with the direct matrix converter.

In most cases, the IMC and sparse matrix converter (SMC) are viewed as having close similarity with the B2B converter because of their common rectifier to inverter arrangement. However, the rectifier and the inverter of the SMCs and IMCs are of complementary types, with the rectifier operating as a current source (CS) while

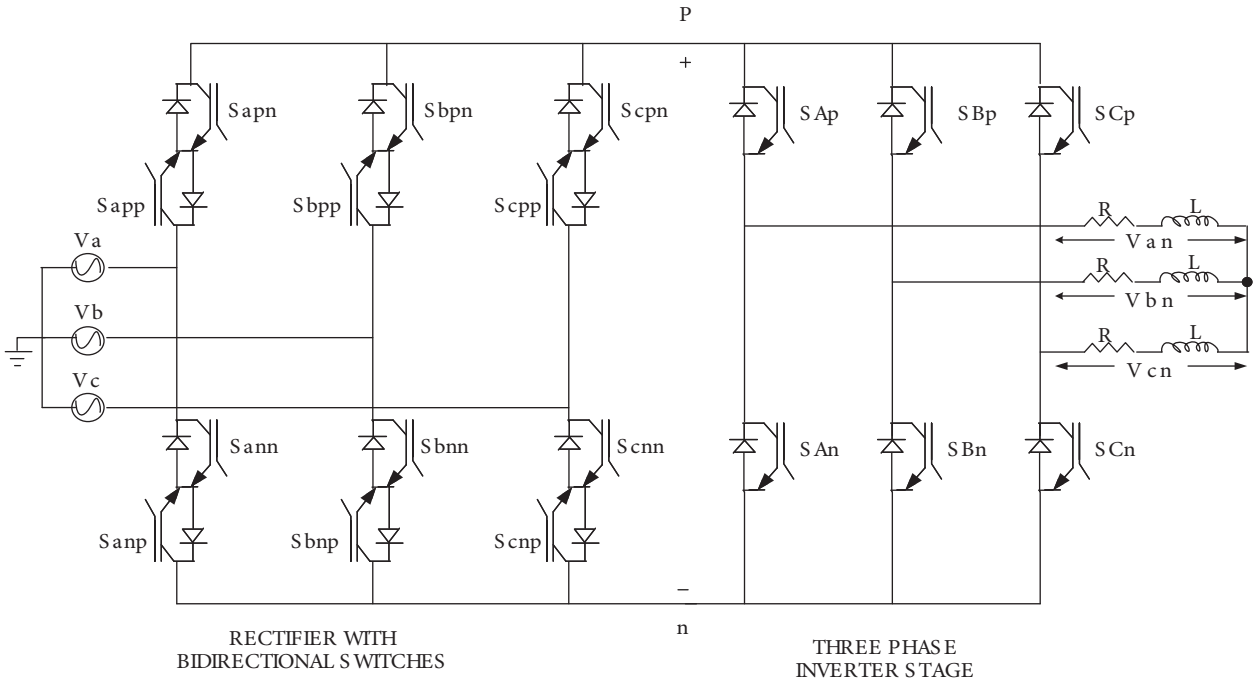

Figure 4. Indirect matrix converter.

the inverter operates as a voltage source (VS). The duo converters are joined at their common fictitious DC link without any passive components, thus leading to a more compact design with a longer lifespan. However, the common voltage gain $\frac{V_o}{V_i}$ of the IMC and SMC is restricted to a maximum value of 0.8660 or $\left(\frac{\sqrt{3}}{2}\right)$, which is certainly not suitable for DG, since this value of voltage supply is usually lower than the anticipated grid

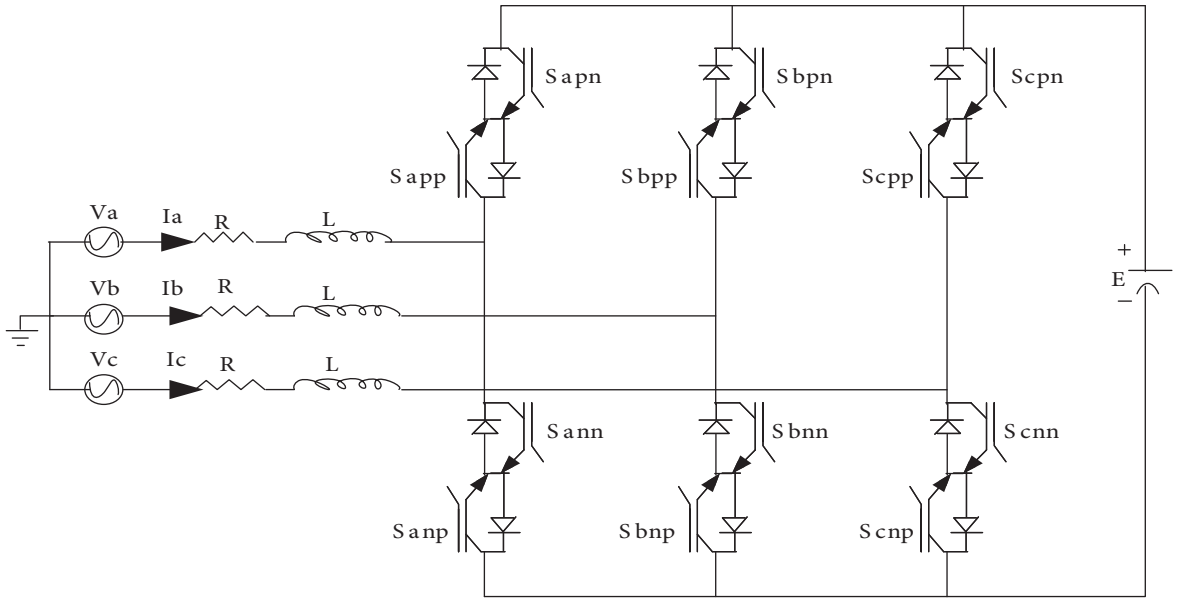

Figure 5. Indirect matrix converter rectifier stage.

voltage [12]. To raise this voltage, a recent recommendation is to add a Z-source LC network to the fictitious DC link of the IMC and SMC, as reported in [13]. In the B2B converter, the input and output voltage boost can be realized with the aid of its large DC link electrolytic capacitor, although this may cause a premature failure despite its high energy density and relatively low price. To extend the lifetime of the converter, a foil capacitor can be used, especially when it is specifically meant to provide filtering rather than storing energy [14]. Regardless of the capacitor type used, the DC capacitor to a large extent demands that an additional sensor and control scheme should be incorporated for regulating its voltage, so as to avoid damage caused by voltage surge, and also to compensate for lower frequency ripples when smaller capacitance is used. In the simulation analysis of this research work, the switching signals presented in Table 4 were used to trigger the 6 bidirectional switches of the three phase thyristor controlled rectifier, while Figure 5 represents the detached rectifier circuit with the bidirectional switches and RL element applied for source harmonic frequency attenuation. Table 5 represents the conventional switching strategy of the three phase voltage source inverter (VSI).

Table 4. Switching signal of IMC bidirectional rectifier switches.

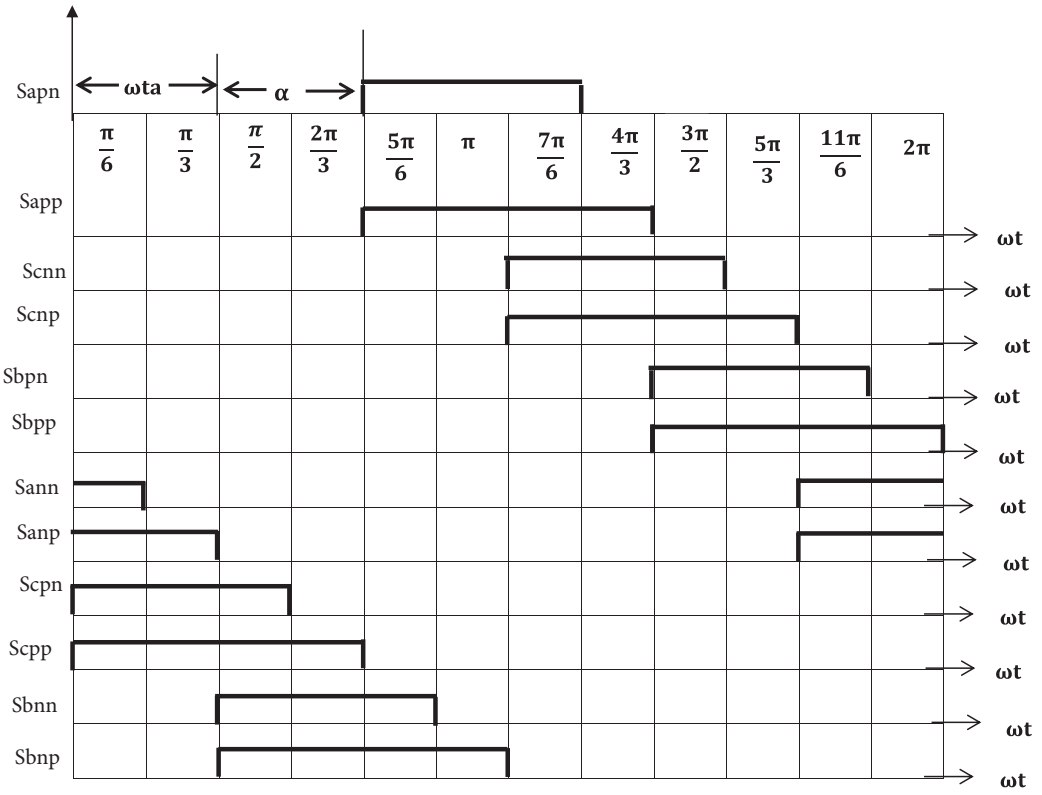

The three phase voltage equations in Eqs. (2)–(4) were derived from Table 2 with the aid of Fourier series analysis:

$$V_{AN} = \sum_{n=1}^{\infty} \frac{2V_d}{n\pi} \sin \omega t; \tag{2}$$

$$V_{BN} = \sum_{n=1}^{\infty} \frac{2V_d}{n\pi} \sin \left(\omega t - \frac{2\pi}{3} \right); \tag{3}$$

$$V_{CN} = \sum_{n=1}^{\infty} \frac{2V_d}{n\pi} \sin\left(\omega t - \frac{4\pi}{3}\right). \tag{4}$$

Table 5. Switching signal of IMC unidirectional inverter switches.

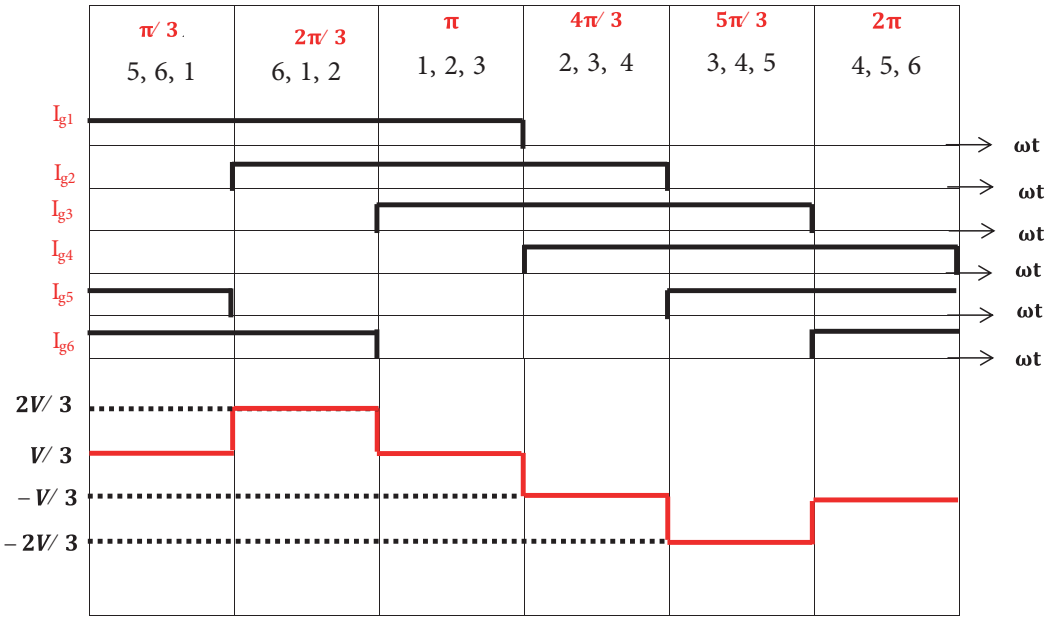

3. Steady state analysis of a three phase 10 HP, 220 V, 50 Hz induction machine

Over the years, induction motors with squirrel-cage rotors have been considered to be the workhorses of most industrial applications because of their low cost of maintenance, rugged construction, good self-starting capability, robustness, and high efficiency value, with availability in the ranges of fractional horse power to multi-megawatt capability [15,16].

Low power machines are available in single phase, while polyphase and multi-megawatt machines are used in adjustable (variable) speed drives with three phase stator and rotor windings [16]. The stator windings are supplied with a balanced three phase AC voltage, which produces induced emf in the rotor windings through transformer action [16]. In the construction process, it is possible to arrange the distribution of stator windings so that there is an effect of multiple poles producing several cycles of magnetomotive force (mmf) around the air gap. This field establishes a spatially distributed sinusoidal flux density in the air gap. The speed of rotation of the field at a very synchronous value is defined by Eq. (5):

$$N_e = N_s = \frac{120f}{p}, \tag{5}$$

where $N_e = N_s =$ synchronous speed in RPS, $f =$ rated frequency in Hz, and $p =$ number of poles.

At the instant of starting an induction motor, its rotor is initially stationary and its conductors are always subjected to a sweeping magnetic field, thus inducing current in the short-circuited rotor at the rated frequency. The interaction of air gap flux and rotor mmf produces torque across the rotor axis. At synchronous speed of the induction motor, when the rotor rotates at a speed equal to the synchronous speed value ($N_{mr} = N_{ms}$), zero torque (no torque) is produced across the rotor axis due to negligible induction and a zero slip value. At a

speed value less than the synchronous speed, the speed differential $(N_{mr} - N_{ms})$, also known as the slip speed, induces rotor current and sets up a torque value, called developed torque, with a corresponding positive slip value [17].

3.1. Induction motor equivalent circuit and mathematical model

A simplified per-phase equivalent circuit model of an induction motor is a valuable tool for the analysis and performance prediction of an induction machine in a steady state condition. This simplified equivalent circuit is shown in Figure 6.

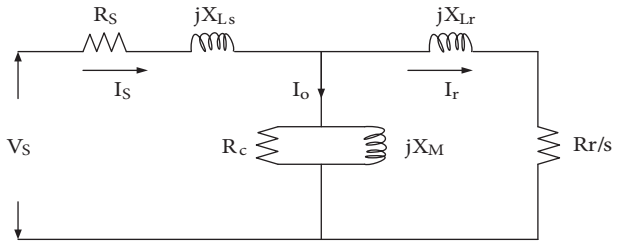

Figure 6. Equivalent circuit of an induction machine.

At standstill, the slip (s) is always one, implying that motor speed at this condition is zero. At synchronous speed of the motor operation, the slip is zero, since speed differential $(N_{mr} - N_{ms})$, also known as the slip speed, is zero. Rotor current and torque at this point are zero. The machine only takes in excitation current I_o.

At any subsynchronous speed with slip values ranging from $0 < s < 1.0$, the rotor current I_R is principally influenced by $\frac{R_r^1}{s}$ and the $\omega_e L_{Lr}$ parameter with $\frac{R_r^1}{s} \gg \omega_e L_{Lr}$ [18].

The performance characteristics of the machine are derived from Eqs. (6)–(20).

$$\text{Stator copper loss } = P_{LS} = 3 \times I_s^2 \times R_s \tag{6}$$

$$\text{Core loss } = P_{LC} = \frac{3 \times V_C^2}{R_C} \tag{7}$$

$$\text{Power across the air gap } = P_g = 3 \times I_r^2 \times \frac{R_r^1}{s} \tag{8}$$

$$\text{Rotor copper loss } P_{Lr} = 3 \times I_r^2 \times R_r^1 \tag{9}$$

$$\text{Output power } = P_{out} = \text{ airgap power } (P_g) - \text{rotor copper loss } (P_{Lr}) \, (10) \tag{10}$$

$$P_{out} = 3 \times I_r^2 \times \frac{R_r^1}{s} - 3 \times I_r^2 \times R_r = 3 \times I_r^2 \times \frac{R_r^1}{s} (1 - s) \tag{11}$$

$$\text{Shaft power: } P_{sh} = P_{out} - P_{fw} \tag{12}$$

Here, P_{fw} = friction and winding loss of the machine. The developed torque is taken from Eq. (13).

$$T_e = \frac{P_o}{\omega_m} \tag{13}$$

$$\omega_m = \frac{2\omega_s}{p}(1-s) \tag{14}$$

$$T_e = 3 \times I_r^2 \times \frac{R_r^1}{s} \times (1-s) \div \frac{2\omega_s}{p}(1-s) = \frac{3 \times p}{2 \times \omega_s} \times I_r^2 \times \frac{R_r^1}{s} \tag{15}$$

From Figure 7, the stator input impedance Z_{in}, stator input current I_{as}, and rotor input current I_{ar} are derived as follows:

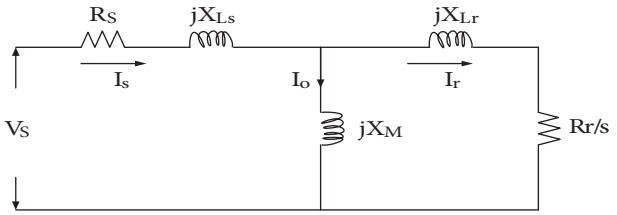

Figure 7. Steady state equivalent circuit of an induction machine.

$$Z_{in} = R_s + jX_{Ls} + \frac{jX_M\left(\frac{R_r^1}{s} + jX_{Lr}^1\right)}{\frac{R_r^1}{s} + j\left(X_{Lr}^1 + X_M\right)} \tag{16}$$

$$I_s = \frac{V_s}{Z_{in}} \tag{17}$$

$$I_r = \frac{jX_M \times I_s}{\sqrt{\left(\frac{R_r^1}{s}\right)^2 + \left(X_{Lr}^1 + X_M\right)^2}} \tag{18}$$

$$I_r^2 = \frac{X_M^2 \times I_s^2}{\left(\frac{R_r^1}{s}\right)^2 + \left(X_{Lr}^1 + X_M\right)^2} \tag{19}$$

The new torque equation is derived from direct substitution of Eq. (19) into Eq. (15) and presented in Eq. (20):

$$T_e = \frac{3 \times p}{2 \times \omega_s} \times \left(\frac{X_M^2 \times I_s^2}{\left(\frac{R_r^1}{s}\right)^2 + \left(X_{Lr}^1 + X_M\right)^2}\right) \times \frac{R_r^1}{s}. \tag{20}$$

When the nth harmonic is injected into the machine, the steady state equivalent circuit changes as shown in Figure 8, where: $V_{s(n)} = \frac{\sqrt{2}V_d}{n\pi}$(21).

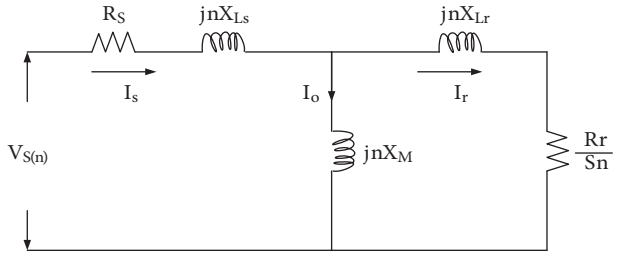

Figure 8. Steady state equivalent circuit of an induction machine with nth harmonic.

The corresponding torque, the stator current, and the net impedance in this condition are given by Eqs. (22)–(24).

$$T_e = \frac{3 \times p}{2 \times \omega_s} \times \left(\frac{n^2 X_M^2 \times I_s^2}{\left(\frac{R_r^1}{s_n}\right)^2 + n^2 \left(X_{Lr}^1 + X_M\right)^2} \right) \times \frac{R_r^1}{s_n} \tag{21}$$

$$I_s = \frac{V_{s(n)} = \frac{\sqrt{2} V_d}{n\pi}}{Z_{in}} \tag{22}$$

$$Z_{in} = R_s + jnX_{Ls} + \frac{jnX_M \left(\frac{R_r^1}{s_n} + jnX_{Lr}^1\right)}{\frac{R_r^1}{s_n} + jn\left(X_{Lr}^1 + X_M\right)} \tag{23}$$

The positive sequence harmonic S_{n1} and negative sequence harmonic S_{n2} are given by Eqs. (25) and (26).

$$S_{n1} = \frac{n - 1 + s}{n} \tag{24}$$

$$S_{n2} = \frac{n + 1 - s}{n}. \tag{25}$$

When $|(R_s + j\omega_e L_{ls})| \ll |(j\omega_e L_m)|$, then the steady state equivalent circuits in Figures 7 and 8 are modified into Figures 9 and 10, respectively.

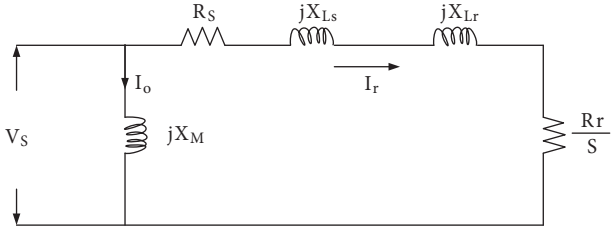

Figure 9. Modified steady state equivalent.

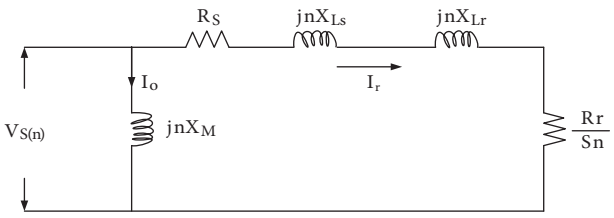

Figure 10. Modified steady state circuit of an induction machine with nth equivalent circuit of an induction harmonic. machine.

The corresponding torque equation for Figure 9 is presented in Eq. (27), while Eq. (28) represents the torque equation for Figure 10.

$$T_e = \frac{3 \times p}{2 \times \omega_s} \times \left(\frac{V_s^2}{\left(R_s + \frac{R_r^1}{s}\right)^2 + \left(X_{Ls} + X_{Lr}^1\right)^2} \right) \times \frac{R_r^1}{s} \tag{26}$$

$$T_e = \frac{3 \times p}{2 \times \omega_s} \times \left(\frac{\left(V_{s(n)}\right)^2}{\left(R_s + \frac{R_r^1}{s_n}\right)^2 + n^2\left(X_{Ls} + X_{Lr}^1\right)^2} \right) \times \frac{R_r^1}{s_n} \tag{27}$$

The torque equation applied in this work was obtained using Thevenin's approach on the rotor axis of Figure 9, due to its precision and computational accuracy. The net Thevenin impedance, voltage, and motor developed torque are represented in Eqs. (29)–(31).

$$Z_{th} = R_{th} + jX_{th} = \frac{jX_M \times (R_s + jX_{Ls})}{R_s + j\left(X_{Ls} + X_M\right)} \tag{28}$$

$$V_{th} = \frac{jX_M \times V_s}{R_s + j\left(X_{Ls} + X_M\right)} \tag{29}$$

$$T_e = \frac{3 \times p}{2 \times \omega_s} \times \left(\frac{V_{th}^2}{\left(R_{th} + \frac{R_r^1}{s}\right)^2 + \left(X_{th} + X_{Lr}^1\right)^2} \right) \times \frac{R_r^1}{s} \tag{30}$$

3.2. Effect of rotor resistance on maximum torque

In a wound rotor induction motor, applied torque is increased by improving the power factor, which is actualized by adding an external resistance in the rotor circuit. However, this resistance addition increases the rotor impedance and thus reduces the corresponding rotor current [19].

At the instant of an appreciable power factor improvement over the current magnitude, the effect of impedance is decreased, hence increasing the starting torque. After a certain change in time, the effects of increased impedance predominate the corresponding effect on the improved power factor, thereby causing a sharp decrease in the applied torque [19].

4. Simulation results and analysis

The results presented in Figure 11 depict the unmodulated staircase voltage for the three phase IMC with the corresponding output current I_o and supply current I_s. Figure 12a depicts phase A output voltage of the modulated IMC; Figure 12b shows phase current, phase voltage, and line voltage of the modulated IMC.

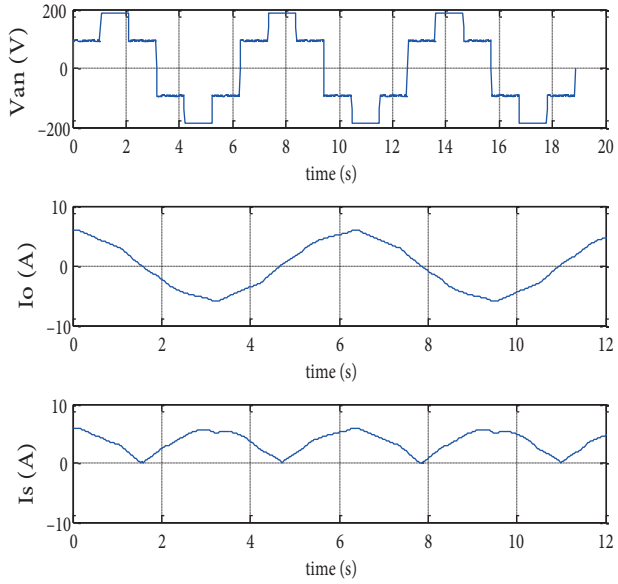

Figure 11. Output voltage and current

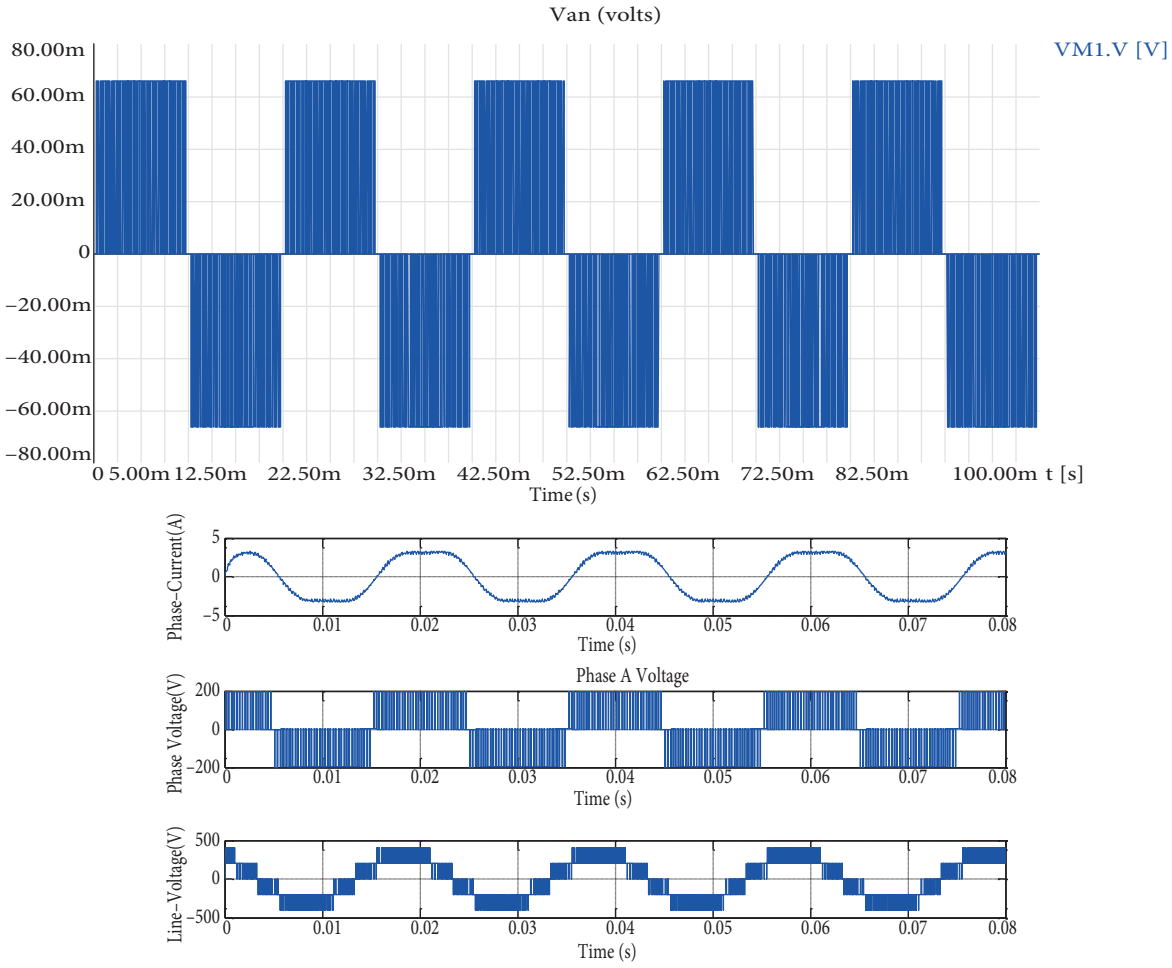

Figure 12. a. Output voltage of phase A b. Phase current, phase voltage,

For a typical induction motor, the torque-speed curve is plotted at varied rotor resistance using the parameters shown in Table 6.

Table 6. Motor simulation parameters.

Motor parameters	Values used
Supply voltage V_s	220 V
Number of poles P	4
Supply frequency F	50 Hz
Varied rotor resistance R_r	0.1 Ω, 0.2 Ω, 0.5 Ω, 1.0 Ω, and 1.5 Ω
Stator resistance R_s	0.4 Ω
Stator leakage reactance X_{Ls}	1.5 Ω
Rotor leakage reactance X_{Lr}	1.5 Ω
Magnetizing reactance X_M	30 Ω

The results obtained for the torque-speed curve are presented in Figures 13–15. Figure 14 depicts the torque-speed characteristics indicating the plugging, motoring, and regenerative regions. The plugging zone is bounded by $-100 \leq \omega_s(rad/s) = 0$, while the motoring zone is bounded by $0 \leq \omega_s\,(rad/s) \leq 152$, and lastly, the regenerative mode is also bounded by $152 \leq \omega_s\,(rad/s) \leq 450$. Similarly, Figure 16 depicts torque-speed characteristics at varied rotor resistance values.

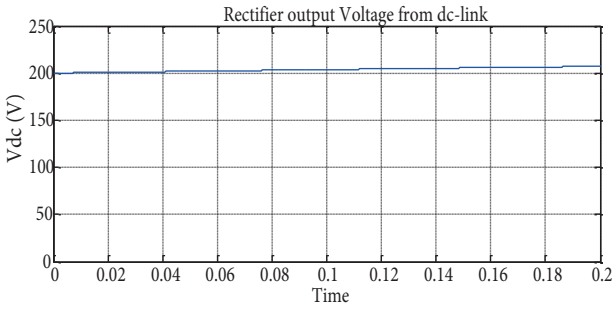

Figure 13. Rectifier output voltage.

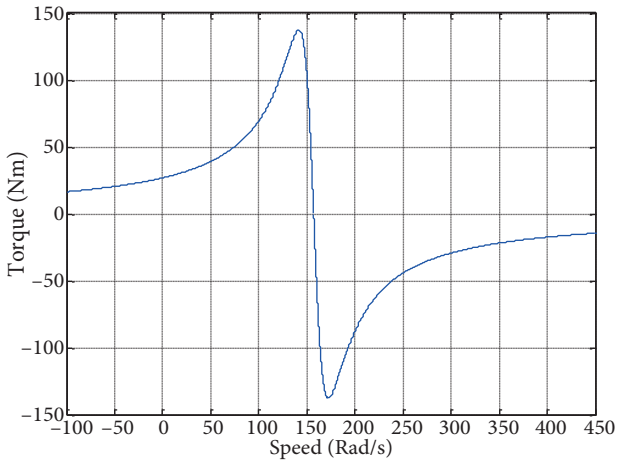

Figure 14. Torque-speed characteristics indicating plugging, motoring, and generative zones.

4.1. Major industrial applications of the indirect matrix converter

The IMC is widely applied in the operation of a slip energy recovery scheme, also known as a static Scherbius drive. In this method, a 3-phase AC supply is connected to the stator terminals. The resultant rotor current is rectified and fed back to the stator input via a line commutated inverter and an ideal large line inductor.

The static Scherbius drive requires that the slip power in the rotor flows in the reverse direction. Therefore, by replacing the ideal diode rectifier with a thyristor controlled bridge rectifier, the slip power is controlled to flow in either direction [20]. Hence, with this reverse slip power flow at subsynchronous speed, the power corresponding to the shaft input (mechanical) power can be pumped out of the stator. It can be shown that such a drive system with bidirectional slip power flow can be controlled in motoring and generating operational

conditions within the subsynchronous and supersynchronous speed ranges. Figure 17 presents a schematic diagram of a slip energy recovery scheme, also called the Scherbius drive. The voltage equations for the AC supply remains the same as those presented in Eqs. (2)–(4) above.

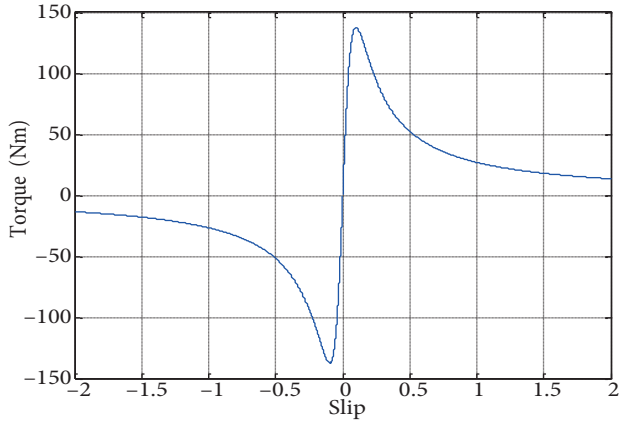

Figure 15. A plot of torque against slip.

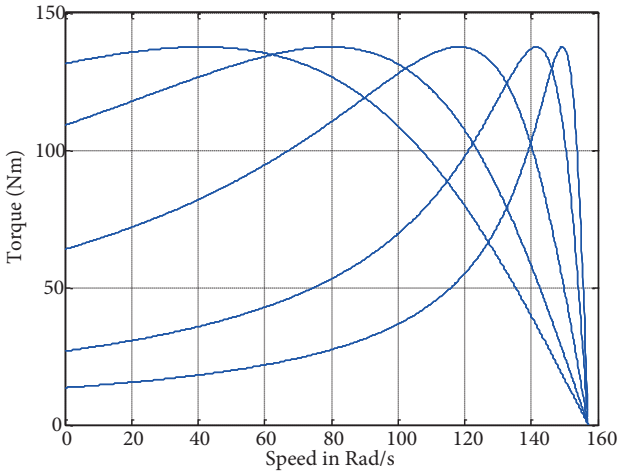

Figure 16. A plot of torque against speed at varied rotor resistance values.

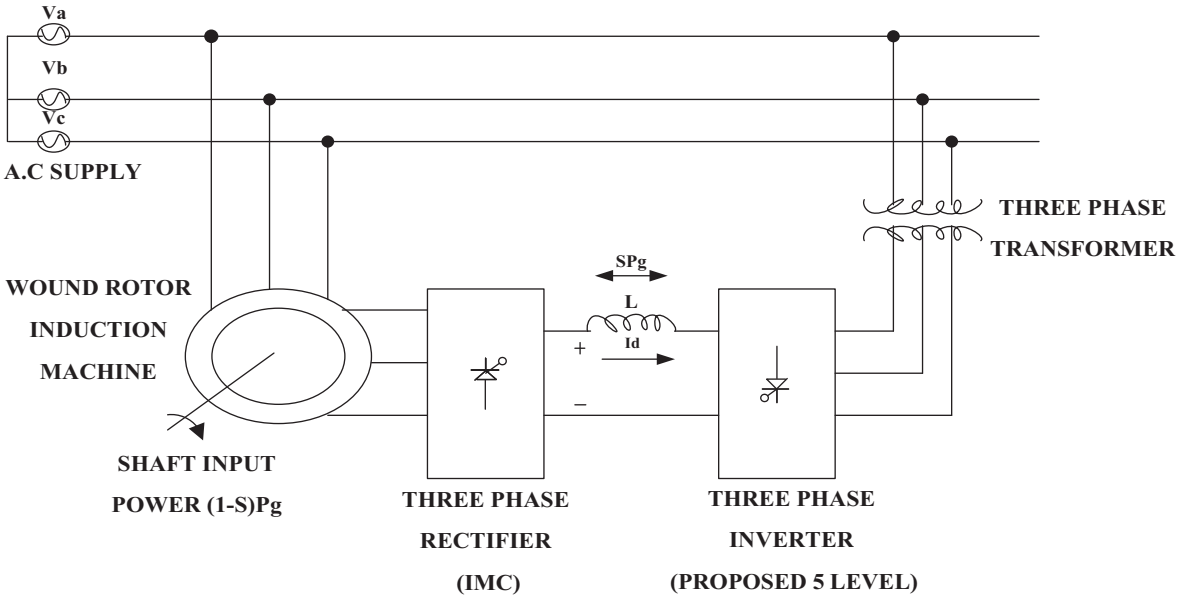

Figure 17. Static Scherbius drive system.

If the motor runs at a given slip value "S" with the internal voltage drop neglected (ideal rotor winding), the line to line rotor output voltage equations are represented by Eqs. (32) to (34).

$$V_{ABr} = \frac{N_r}{N_s} \times S \times V_{ml} \sin \omega_r t \tag{31}$$

$$V_{BCr} = \frac{N_r}{N_s} \times S \times V_{ml} \sin\left(\omega_r t - \frac{2\pi}{3}\right) \tag{32}$$

$$V_{CAr} = \frac{N_r}{N_s} \times S \times V_{ml} \sin\left(\omega_r t - \frac{4\pi}{3}\right) \tag{33}$$

Here, N_r stands for the number of turns in the rotor windings, N_s stands for stator number of turns, and S stands for the slip, which is the difference in synchronous speed and motor speed, all divided by the synchronous speed value. All other variables are already known in accordance with voltage equations.

The average value of the rectifier output voltage is obtained from Eq. (35):

$$V_{od} = \frac{N_p \times V_{ml}}{\pi} \sin\left(\frac{\pi}{N_p}\right) \cos\alpha \tag{34}$$

N_p represents the number of rectifier pulses, which in this context is 6. V_{ml} is the rotor line to line voltage amplitude. α is the converter control delay angle, which is always 0 for an ideal diode.

Practically, α is always taken as a second quadrant angle between $90 \leq \alpha \leq 180$, so that the controlled rectifier operates in inversion mode, thereby enhancing the supply of slip power back to the AC source [20,21].

The torque developed and the rotor dissipated power are as presented in Eqs. (6)–(20) above, respectively.

A simulation was carried out to determine the dynamic and steady state performance of the wound rotor induction machine that forms an integral part of the static Scherbius drive, as well as the rectified three phase inverter output voltage achieved with the aid of the inductive shunt transformer. The results presented in Figures 18–22 represent the d-q axes' voltages and currents for the stator and rotor windings, the rotor speed and torque produced by the machine, and the rectified inverter output voltage. Parameters used for this simulation are presented as follows: supply voltage V_s = 200 V; stator resistance R_s = 0.4 Ω; rotor resistance R_r = 0.2 Ω; stator and rotor leakage inductances $L_{Ls} = L_{Lr}$ = 0.0048 H; magnetizing inductance L_m = 95.5 mH; Motor inertia J = 0.025 kgm^2; coefficient of frictional factor B = 0.0008; N.M.S. nominal machine power = 10 HP (7.5 kW); number of poles = 4; operating frequency = 50 Hz; synchronous speed = 1500 rpm.

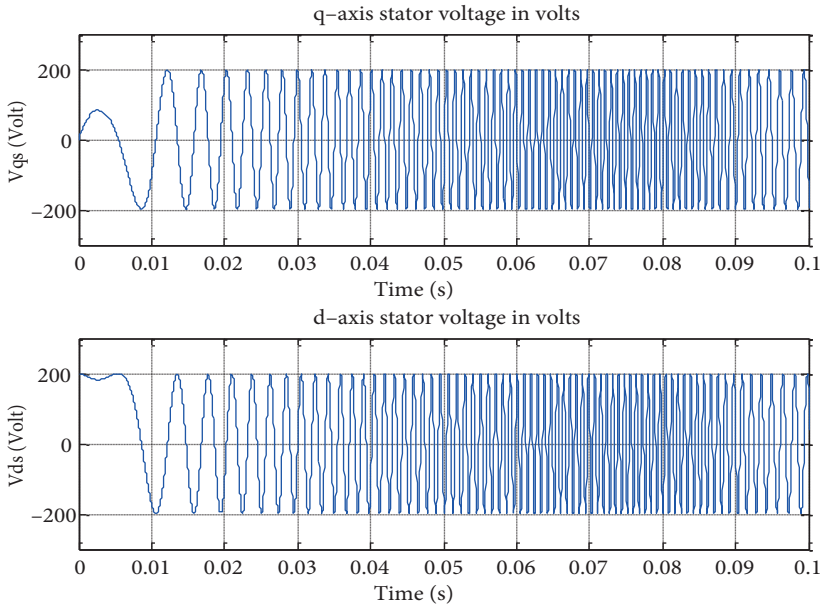

Figure 18. q-d axes' stator voltage.

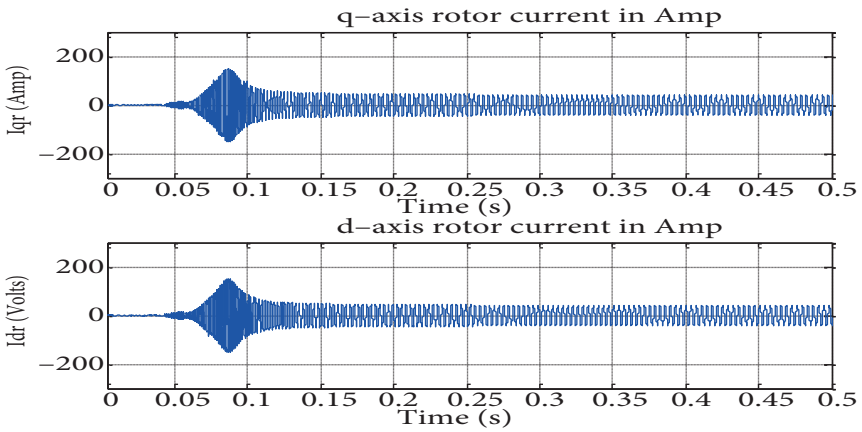

Figure 19. q-d axes' rotor current.

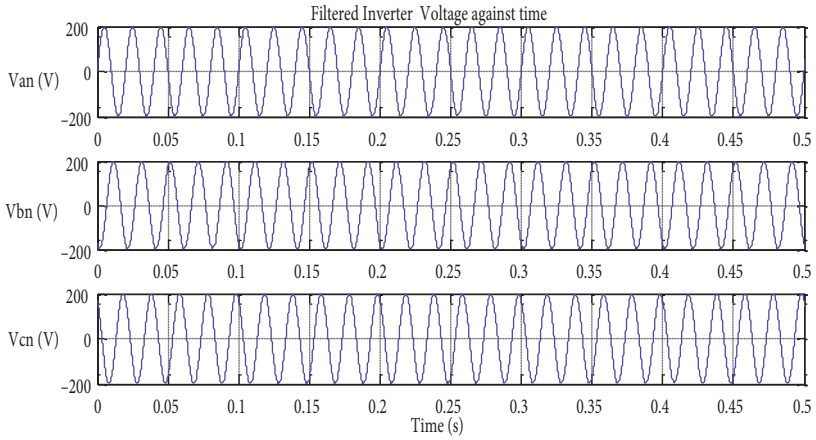

Figure 20. q-d axes' rotor voltage.

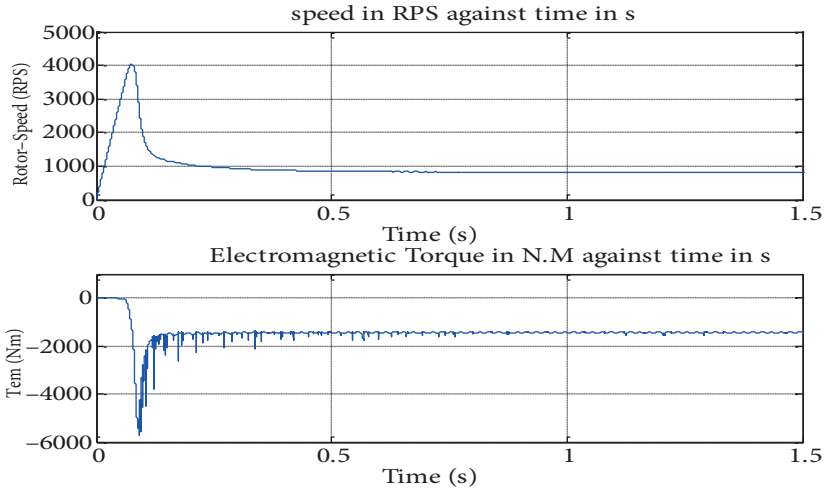

Figure 21. Rotor speed and torque.

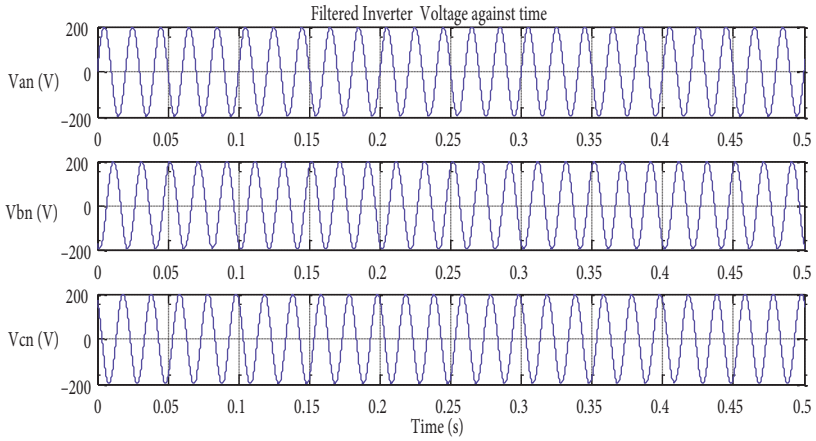

Figure 22. Three phase inverter filtered voltages.

4.2. Conclusion

Considering the motoring region of the torque slip curve of Figure 14, if the point of maximum torque is made to intersect the torque axis, the entire motoring region is observed to be linear. This implies that the ratio of rotor resistance to leakage reactance is set very high $(R_2 \gg X_2)$, such that the induction motor operates in the linear region. A conventional method of obtaining higher resistance is using a conductor with a smaller cross-sectional area or a low value diameter due to the inverse proportionality relation between resistance and area of the conductor.

In the normal motoring region, torque is always set to a zero value when the slip of the machine is zero. As the slip increases with a corresponding decrease in speed, torque increases in a quasilinear curve until a breakdown or maximum torque T_{max} is reached. In this region, the stator drop becomes very small with the air gap flux remaining almost constant due to a well-adjusted value of the IMC control delay angle of Figure 5. Beyond the breakdown torque region, T_e decreases with a proportionate increase in the slip value, as shown in Figures 14 and 15, respectively.

In the plugging region, the rotor rotates in the opposite direction to the air gap flux such that the slip $s > 1$. This condition may arise if the stator supply (phase sequence) is reversed by adjusting the control delay angle of the IMC beyond 90° when the rotor is set in motion, or due to an overhauling type of loading condition that drives the rotor in the opposite direction. Since the torque at this condition is positive with a negative speed value, the plugging torque appears as a breaking torque that is dissipated in the form of energy within the machine, thus causing excessive heating of the machine.

In the regenerative region, the machine acts as a generator. The rotor moves at a supersynchronous speed in the same direction as the air gap flux, thereby making the slip negative, thus creating a negative torque called regenerative torque. The negative slip corresponds to the negative equivalent resistance $\frac{R_r^{'}}{S}$, which generates and supplies energy back to the source, while the positive resistance $\frac{R_r^{'}}{S}$ consumes energy during the motoring operation.

Conclusively, the plugging region depicted in Figure 14 is bounded by $-100 \leq \omega_s \leq 0 rad/s$, which conforms to the negative speed value discussed earlier. The motoring region bounded by $0 \leq \omega_s \leq 152 rad/s$ is set within the prescribed synchronous speed value of $157.08 rad/s$ or 1500 rpm. The regenerative mode bounded by $152 \leq \omega_s \leq 450 rad/s$ has a maximum speed limit greater than the synchronous speed of $157.08 rad/s$ or 1500

rpm, which also conforms to the theoretical convention thereof. Hence, for more efficient drive performance, a three phase source of higher IMC voltage level is applied at the stator terminal to enhance an optimum drive strategy of the above-discussed machine. The simulation result presented in Figure 21 depicts the operation of the machine in the subsynchronous regeneration mode on attainment of a steady state condition in 0.25 s. This is because the shaft, as shown in Figure 17, is being driven by the load with the mechanical energy converted into electrical energy, and also pumped out of the stator with a negative torque of about –1800 Nm. The mechanical power input to the shaft P_m increases as the motor speed rises from 0 to 4000 rps between a time interval of 0 to 0.1 s, with a corresponding decrease in slip that conforms to Eqs. (11) and (12). Under this condition, negative power is fed to the rotor via the cycloconverter. In a time interval of 0.3 s, the motor speed attains a steady state condition at a subsynchronous value of 950 rps, thereby raising the slip value to 0.3667. This mode of operation is typical of a variable-speed wind generation system.

The outcome of the study, in a nutshell, shows that proper voltage and frequency control was achieved through a controlled thyristorized B2B converter. Evaluation of machine performance at varied load conditions when driven by a well-modulated converter was achieved at reduced harmonics.

References

[1] Bueno EJ, Cobreces S, Rodriguez FJ, Hernandez A, Espinosa F. Design of a back-to-back NPC converter interface for wind turbines with squirrel-cage induction generator. IEEE T Energy Conver 2008; 23: 932-945.

[2] Yao J, Li H, Liao Y, Chen Z. An improved control strategy of limiting the dc- link voltage fluctuation for a doubly fed induction wind generator. IEEE T Power Electr 2008; 23: 1205-1213.

[3] Kolar JW, Friedli T, Rodriguez J, Wheeler P. Review of three-phase PWM AC-AC converter topologies. IEEE T Ind Electron 2011; 58: 4988-5006.

[4] Zanchetta P, Wheeler P, Clare J, Bland M, Empringham L, Katsis D. Control design of a three-phase matrix-converter-based ac-ac mobile utility power supply. IEEE T Ind Electron 2008; 55: 209-217.

[5] Bose BK. Power Electronics and AC Drives. Englewood Cliffs, NJ, USA: Prentice Hall, 2002.

[6] Friedli T, Kolar JW, Rodriguez J, Wheeler P. Comparative evaluation of three-phase AC-AC matrix converter and voltage DC-link back-to-back converter systems. IEEE T Ind Electron 2012; 59: 4487-4510.

[7] Kumar V, Joshi RR, Bansal RC. Optimal control of matrix-converter-based WECS for performance, enhancement and efficiency optimization. IEEE T Energy Conver 2009; 24: 264-273.

[8] Wheeler P, Rodriguez J, Clare J, Empiringham L, Weinstein A. Matrix converters: a technology review. IEEE T Ind Electron 2002; 49: 276-288.

[9] Kolar JW, Schafmeister E, Round SD, Ertl H. Novel three-phase AC-AC sparse matrix converters. IEEE T Power Electr 2007; 22: 1649-1661.

[10] Hojabri H, Mokhtari H, Chang L. A generalized technique of modeling, analysis and control of a matrix converter using SVD. IEEE T Ind Electron 2011; 58: 949-959.

[11] Wei L, Lipo TA, Chan H. Matrix converter topologies with reduced number of switches. In: IEEE 2006 Power Electronics Specialists Conference; 18-22 June 2006; Jeju, South Korea. Piscataway, NJ, USA: IEEE. pp 57-63.

[12] Liu C, Loh PC, Wang P, Blaabjerg F, Tang Y, Al-Ammar EA. Distributed generation using matrix converter in reverse power mode. IEEE T Power Electr 2013; 28: 1072-1082.

[13] Kolar JW, Schafmeister E. Novel modulation schemes minimizing the switching losses of sparse matrix converters. In: IEEE 2003 29th Industrial Electronics Society Conference; 2–6 November 2003; Roanoke, VA. Piscataway, NJ, USA: IEEE. pp. 2085-2090.

[14] Wei L, Matsushita Y, Lipo TA. Investigation of dual-bridge matrix converters operating under unbalanced source voltages. In: IEEE 2003 34th Power Electronic Specialists Conference; 2–6 November 2003; Roanoke VA. Piscataway, NJ, USA: IEEE. pp. 2078-2084.

[15] Lavi A, Polge RL. Induction motor speed control with static inverter in the rotor. IEEE T Power Ap Syst 1966; 85: 76-84.

[16] Hori T, Nagase H, Hombu M. Induction motor control systems. In: Wilamowski, BM, Irwin JD, editors. Industrial Electronics Handbook. Boca Raton, FL, USA: CRC Press, 1997. pp. 310-315.

[17] Smith GA. Static Scherbius system of induction motor speed control. IEEE T Power Electr 1977; 124: 557-565.

[18] Weiss HW. Adjustable speed AC drive systems for pump and compressor applications. IEEE T Ind Appl 1974; 10: 157-162.

[19] Fitzgerald AE. Electric Machinery. 5th ed. New York, USA: McGraw-Hill, 1990.

[20] Pena R, Clare JC, Asher GM. Doubly fed induction generator using back-to-back PWM converters and its application to variable speed wind energy generation. IEE P-Elect Pow Appl 1996; 143: 234-240.

[21] Barnes M, Dimeas A, Engler A, Fitzer C, Hatziargyriou N, Jones C, Papathanassiou S, Vandenbergh M. Microgrid laboratory facilities. In: International Conference on Future Power Systems; 16–18 November 2005; Amsterdam, the Netherlands. Piscataway, NJ, USA: IEEE. pp. 1-6.